Monitoring spinach shelf-life with hyperspectral image through packaging films

M.A. Lara , L. Lleó , B. Diezma-Iglesias , J.M. Roger , M. Ruiz-Altisent

A B S T R A C T

Different procedures for monitoring the evolution of leafy vegetables, under plastic covers during cold storage, have been studied. Fifteen spinach leaves were put inside Petri dishes covered with three different plastic films and stored at 4 °C for 21 days. Hyperspectral images were taken during this storage. A radiometric correction is proposed in order to avoid the variation in transmittance of the plastic films during time in the hyperspectral images. Afterwards, three spectral pre-processing procedures (no preprocess, Savitsky–Golay and Standard Normal Variate, combined with Principal Component Analysis) were applied to obtain different models. The corresponding artificial images of scores were studied by means of Analysis of Variance to compare their ability to sense the aging of the leaves. All models were able to monitor the aging through storage. Radiometric correction seemed to work properly and could allow the supervision of shelf-life in leafy vegetables through commercial transparent films.

1. Introduction

The consumption of fresh ready-to-eat products and minimally processed foods has increased in recent years (Artes et al., 2009). Ready-to-eat vegetables have a shelf-life between 7 and 14 days (Garcia Gimeno et al., 1997), depending on the type of vegetable, due to microbiology degradations and the loss of physical and organoleptic properties (Toivonen and Brummell, 2008).

The industry demands objective, non destructive and low cost methods to sense the evolution of this product during storage and to evaluate new systems that have been introduced in the ready-to-use processes as UV-C radiations, O_3 treatments, etc.

Modified atmosphere packaging (MAP) is an essential technology for the success of fresh-cut produce. Polymeric films are a key element in MAP. The most commonly used packaging films are a few plastic polymers: polyolefins (polyethylene and polypropylene), vinyl compound polymers (polystyrene and polyvinyl chloride), and polyethylene terephthalate (polyester). For fresh fruits and vegetables, the films need to be "breathable" because the fresh produce inside is still "alive" and "breathing". Micro perforated films are a good solution for this kind of fresh food.

Hyperspectral imaging allows the acquisition of the spectrum of each pixel, in a specific wavelength range, and generates a spatial map of spectral variations. It is a fast, simple and non destructive technology (ElMasry and Sun, 2010). However, the images obtained are very complex to manage directly and need to be preprocessed and then processed (Fernandez Pierna et al., 2009). Hyperspectral imaging has been used on different applications for the characterization of food quality (Cubero et al., 2011; Du and Sun, 2006; Gowen et al., 2007; Sun et al., 2010) or food safety (Del Fiore et al., 2010; Yao et al., 2008). Regarding vegetables Siripatrawan et al. (2011) used hyperspectral imaging for the detection of Escherichia coli contamination in packaged fresh spinach.

Previous research has been done to compare pre-processing methods for scatter correction in spectra: multiplicative scatter correction (MSC), inverse MSC, extended MSC (EMSC), de-trending, standard normal variate (SNV), normalization and spectral derivatives (Fearn et al., 2009; Laxalde et al., 2011; Rinnan et al., 2009; Zeaiter et al., 2005; Zeaiter and Rutledge, 2009). Geometric preprocessing methods are widely carried out to correct spectral data from drift in baseline, non-linearity, curvilinearity, as well as additive and multiplicative effects. All pre-processing techniques have the goal of reducing the un-modeled variability in the data in order to enhance the performance of the model of prediction. However,

the application of a wrong or too severe type of pre-processing, can remove valuable information. Pre-processing should maintain or decrease the effective model complexity and enhance the model performance.

The objective of the present research was to compare different pre-processing procedures applied to hyperspectral images, regarding their ability to monitor the evolution and spoilage of leafy vegetables under plastic covers during storage. First, the effect of the variation in transmittance of the plastic films that cover the leaves in the measurements was established and corrected. Second, three pre-processing procedures: (a) no pre-process, (b) Savitsky Golay (SG), and (c) Standard Normal Variate (SNV) combined with principal component analysis (PCA), were applied and compared.

2. Materials and methods

Three groups of leaves ($n = 5$ leaves per group) were randomly selected from bags acquired in a local market. Three micro perforated plastic films (polypropylene PPLUS® 160, P1; polypropylene PPLUS® 190, P2; and biaxially oriented polypropylene 30 μm, P3) commonly used in the packing industry of vegetables, were selected. Each group of leaves was assigned one type of plastic film. Each leaf was individually left inside a Petri dish with a piece of grey plastic and covered by the corresponding plastic film. The samples were stored at 4 °C during the whole measurement period. Hyperspectral images were acquired 7 times through 21 days: at 0, 4, 7, 11, 14, 18 and 21 days.

Hyperspectral vision system consisted of a CCD camera with a VNIR spectrometer (Headwall Photonics Hyperspec™) working between 400 and 1000 nm. It was equipped with a progressive line-by-line scan spectrograph with a slit of 25 μm. The selected spectral resolution was 3.2 nm (189 wavelengths), and the spatial resolution was 0.26 mm/pixel. One halogen lamp was used for the illumination. Specific software, Headwall Hyperspec™, was used to control the equipment. Images were acquired according to the conditions shown in Table 1. Samples were scanned acquiring the whole surface of the leaf. A hypercube dataset was obtained from each image.

Relative reflectance hyperspectral images were computed simultaneously to the acquisition, by the software of the camera. White reference (barium sulfate) and dark current signal (acquired with the objective of the camera covered by a black tap) were acquired before each batch of images. Then, each line of the image was corrected pixel by pixel subtracting the dark current and dividing this result by the white reference minus the dark current.

Aiming to obtain a calibration data set completely independent on the validation data set, the 15 leaves were separated into two different groups: a calibration set with three leaves of each plastic, and a validation set with the remaining two leaves of each plastic. The average spectrum of each leaf of the calibration set was computed from the hyperspectral images. Each average spectrum was computed considering all the pixels belonging to the leaf; depending on the size of the leaf the number of spectra range from $n = 7293$ to 85702 (original images without reduction of the spatial resolution). Calibration data set was formed by 63 average spectra (3 leaves × 3 films × 7 dates). Models were generated with the calibration data set. Two types of validations were performed: (a) one applying the models to all the pixels of the leaves of the validation set and (b) a second one considering also all the pixels of the leaves of the calibration set.

Table 1
Configuration of the image acquisition conditions

Spectral binning	4 (189 Wavelengths)
Frames to average	5
Scan length	140 mm
Slit	25 μm
Exposition time	80 ms

2.1. Preprocessing procedures

All the processes described in this section were applied to the calibration set of spectra and also to all the pixels of the hyperspectral images.

2.1.1. Radiometric correction

Radiometric correction (RC) is currently employed in remote sensing for overcoming changes in the measured light due to the atmospheric transmittance and the position of the sun (Sims and Gamon, 2002; Song et al., 2001). In the present study, this correction was used to correct the measured signal for variation in plastic film transmission. A piece of grey plastic of 25 × 25 mm, having a global reflectance similar to a leaf, was inserted in each Petri dish, beside the spinach leaf.

Let be:

- two pixels of grey plastic (position a) and of leaf (position b);
- $S_0(a, t)$ and $S_0(b, t)$ the measured signal from the two pixels a and b on the white reference before the measurement made at date t.
- $F(a, t)$ and $F(b, t)$ the internal gain factor of pixels a and b.
- $I_0(a, t)$ and $I_0(b, t)$ the intensity of the input light for the two positions a and b at date t.
- $P(t)$ the transmission of the plastic film, at date t, supposed independent of the position.
- G the reflectance of the grey plastic supposed independent of the position and the date.
- $R(b, t)$ the reflectance of the leaf at pixel b and date t.

Fig. 1 illustrates the light path for the two pixels during the measurement. The signals finally collected by the camera are given by:

$$S(a,t) = I_0(a,t) \cdot P(t)^2 \cdot G \cdot F(a,t) \text{ and } S(b,t) = I_0(b,t) \cdot P(t)^2 \cdot R(b,t) \cdot F(b,t)$$

However, assuming a unitary reflectance for the white reference, we have:

$$S_0(a,t) = I_0(a,t) \cdot F(a,t) \text{ and } S_0(b,t) = I_0(b,t) \cdot F(b,t)$$

Then, the values collected for the two pixels are:

$$X(a,t) = S(a,t)/S_0(a,t) = P(t)^2 \cdot G \text{ and } X(b,t) = S(b,t)/S_0(b,t) = P(t)^2 \cdot R(b,t)$$

The average value of $X(a, t)$ was computed over all the pixels of the grey plastic and then divided by the value of G measured before the experiment, yielding an estimation of $P(t)^2$. Each pixel b of the leaf was then divided by this quantity, giving an estimation of the true reflectance $R(b, t)$.

2.1.2. Multiplicative and additive effect

Savitsky–Golay smoothing and differentiation algorithm (SG) was applied to the spectra: a polynomial of order three was fitted to 21 wavelengths width and the second derivative function was applied to the smoothed spectra.

After SG algorithm, the multiplicative effect was corrected by Standard Normal Variate scaling (SNV). SNV subtracts to each wavelength of the spectrum (λ_i) the mean value of this spectrum

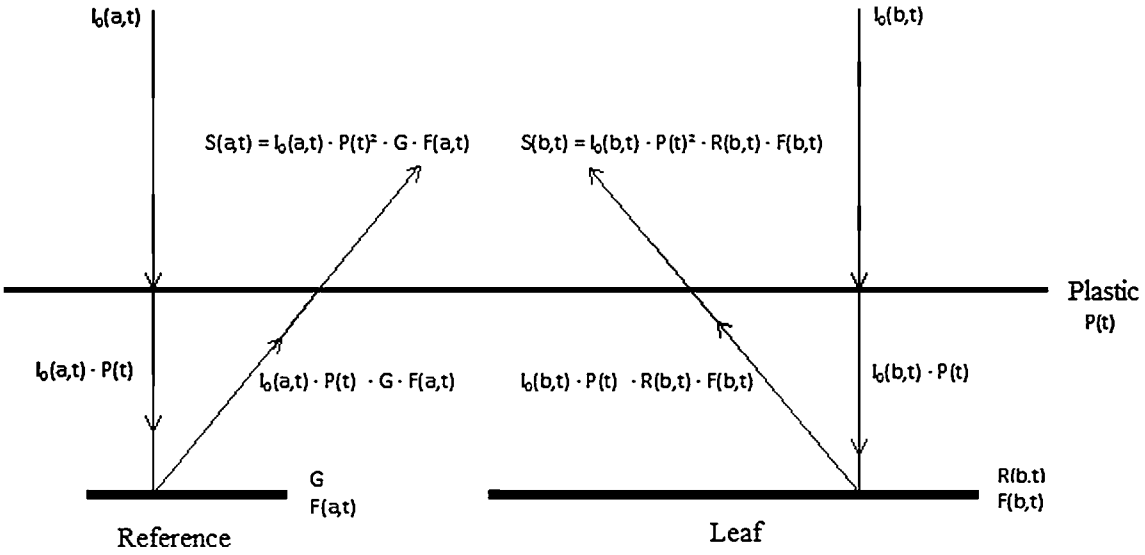

Fig. 1. Light modifications between source and camera detector for the two pixels (a = reference, b = leaf) considering date t. Io(a, t) and Io(b, t) = intensity of the input light for the two positions a and b, at date t. P(t) = transmission of the plastic film, at date t. F(a, t) and F(b, t) = internal gain factor of pixels a and b. G = reflectance of the reference. R(b, t) = reflectance of the leaf at pixel b and date t.

(λ_m) and divides it by the standard deviation of this spectrum (STD). Resulting spectra have a unit standard deviation and a mean equal to zero.

$$\lambda_{i\_SNV} = (\lambda_i - \lambda_m)/\mathrm{STD}$$

2.2. Data processing

Several principal component analyses (PCA) were computed on the calibration set of average spectra of the selected leaves (n = 63), in which the following pre-processes were successively performed: (a) radiometric correction; (b) radiometric correction and SG algorithm and (c) radiometric correction, SG algorithm and SNV. The resulting loadings of the PCA obtained from the spectra processed with these three procedures (a, b and c) were used for the projection of the corresponding corrected hyperspectral images with the aim to monitor the evolution of the surface of each leaf during time. Three virtual images of scores were obtained from such projections for each leaf, one per each different pre-processing method. The projections were carried out on images with a reduction of the spatial resolution (from 0.26 mm/pixel to 1.04 mm/pixel), in order to reduce the computation time.

The scores of the artificial images were studied by means of analysis of variance in order to compare the pre-processing procedures for the detection of the evolution of the leaves and the influence of each plastic film in the preservation of the quality and freshness.

In order to test the best pre-processing procedure for sensing the aging of the leaves, the pixels of the leaves were pooled together for the first day (first group) and for the last day (second group). ANOVA's were carried out for each of the three pre-processing procedures comparing these two groups. For an accurate comparison of the ANOVA results, the same number of pixels, randomly selected per group was considered for (a) calibration set (n = 31.000 per group), (b) validation set (n = 17.000 per group) and (c) calibration plus validation set (n = 48.000 per group). Consequently, nine ANOVÁs were calculated (3 sets of data × 3 pre-processing procedures).

In order to evaluate the ability of the plastic films to preserve the quality of the leaves, additional ANOVÁs were calculated for hyperspectral images in which only RC had been applied. For each plastic film separately, pixels of the leaf images were pooled together for the analysis, categorized in two extreme groups: leaves from the first day and leaves from the last day. The analyses were carried out on the calibration set and on the validation set. Same number of pixels, randomly selected, were considered on each plastic for an accurate comparison of ANOVA results (Calibration set n = 7.400 per group, Validation set n = 3.900 per group).

Finally, in order to analyze the evolution rates of the leaves, ANOVÁs were computed on each individual leaf from calibration and validation sets, comparing the same number of pixels on each leaf, (n = 800 per group, randomly selected). Only hyperspectral images with RC were considered in these ANOVA's.

3. Results

3.1. Radiometric correction

The effect of the radiometric correction can be seen in Fig. 2, where all the average spectra of the leaves were plotted (n = 105), before correction (upper left) and after RC (lower left). Without correction, a strange trend in some spectra could be observed: five spectra showed higher level of intensity at NIR range (higher than 700 nm) compared with the rest of the average spectra. A PCA was calculated and the corresponding scores were analyzed (Fig. 2, upper right); the same five samples appeared separated from the rest of the population. These five outlier spectra corresponded to the five leaves of plastic 1 on the last date. The hypothesis is that plastics suffered changes on their structure and composition through the 21 days. After RC, these five spectra were completely corrected and did not appear anymore as outliers in the PCA plot (Fig. 2, lower right). In addition, the average RC spectra at NIR region was more scattered than in non RC spectra.

3.2. Spectroscopy comments

3.2.1. Reflectance spectra with the radiometric correction

PCA was computed on radiometric corrected spectra (n = 63). First and second components were not related to the time evolution (data not shown), probably because they were more related to un-modeled variability of spectra/images such geometric effects or light variations. The third principal component (PC3) sensed the evolution of the leaves.

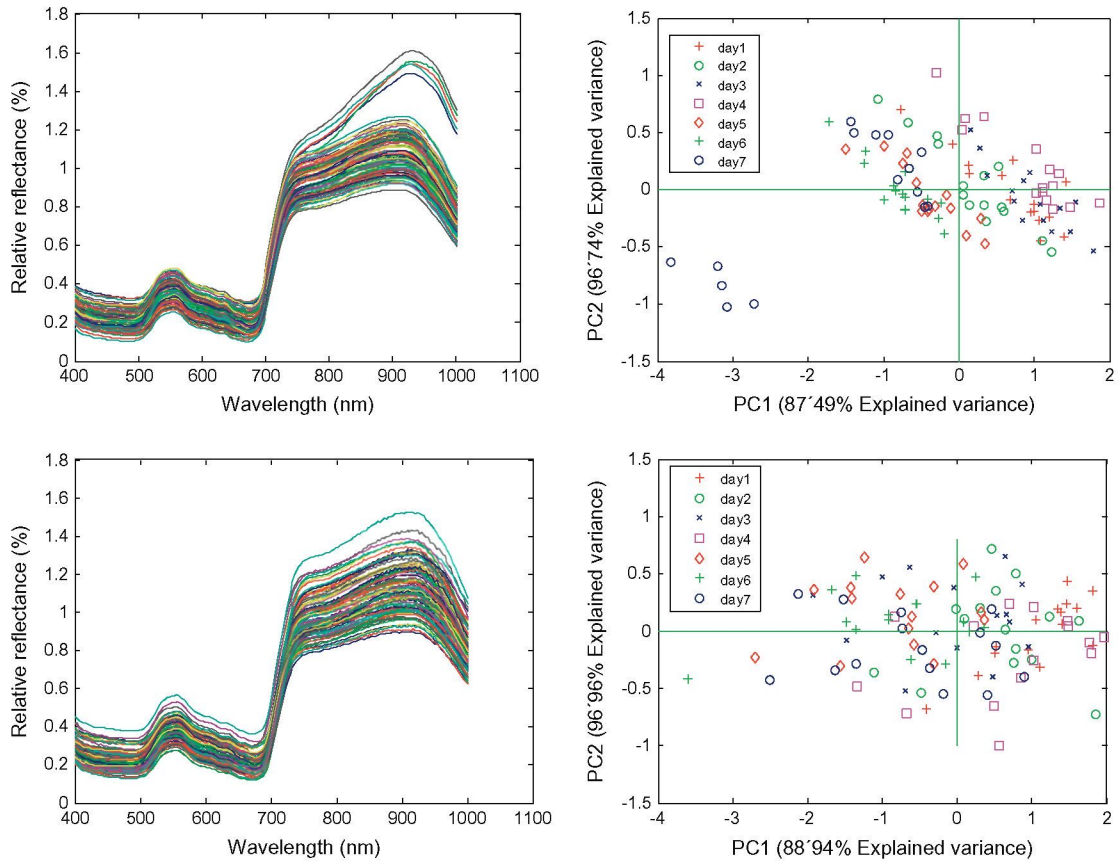

Fig. 2. Upper left: raw mean spectra of the leaves ($n = 105$) without radiometric correction. Upper right: scores of the PC1 vs. PC2 from PCA on raw mean spectra. Lower left: mean spectra of the leaves after the radiometric correction. Lower right: scores of the PC1 vs. PC2 from PCA on mean spectra after radiometric correction.

The global shape of the spectra can be observed in Fig. 3 (upper left)[1]. This is the typical shape of a plant leave spectra (Siripatrawan et al., 2011; Xue and Yang, 2009) in which three main regions can be recognized: the "red edge" region between 680 and 740 nm approximately, a reflectance peak in the green region (500–600 nm), and a broad region at NIR with a high level of reflectance.

Fig. 3 also shows that the global reflectance of the mean spectrum of each plastic on the last day was higher than the corresponding for the first day. That could be due to the changes in the structure and composition of the leaf along time (Jacquemoud and Baret, 1990). This phenomenon has already been described by several authors (Asner, 1998; Liy et al., 2010): when the plant leaves are aging, there is a decrease in the content of chlorophyll, and of other foliar pigments. Besides, water content decreases, which can produce an increase in the content of air between cells; consequently, the scattering increases. As a result, the global reflectance increases in all the visible range and mainly in the near infrared regions.

Fig. 3 (lower left), shows the loadings of PC3, related to the evolution of leaves during storage. The following parts can be observed: a first part in the visible range with negative values (between 400 and 500 nm) which is associated with the blue color, and a second region with positive values (between 500 and 650 nm) which is associated with green and yellow colors. Therefore, it could be concluded that during the storage period, the blue coloration of the leaves decreases, whereas the green and yellow colorations increase.

Gitelson et al. (2006) described a conceptual model capable of estimating total chlorophylls, carotenoids and anthocyanins contents in leaves from many tree and crop species. They show different range of wavelengths maximally sensitive to absorption by the pigment of interest (Table 2). Anthocyanin absorbs around 550 nm, consequently in leaves with anthocyanins only the region around 700 nm is used to estimate chlorophyll content, while in leaves without anthocyanins two regions of the spectra are sensitive to the content of chlorophyll (540–560 nm and 690–720 nm). These authors proposed an estimation of chlorophyll content in leaves free of anthocyanin based on the ratio of the reflectance in NIR range and the reflectance at 540–560 nm. According to Pavia et al. (2007), major pigments in spinach leaves are chlorophyll a and b and carotenoids, and then it could be feasible to consider the cited ratio. Fig. 3 (upper right) shows the radiometric corrected average spectra which has been mean centered, in order to improve the visualization of the changes that occurred in the cited ratio. It can be observed that this ratio increases during the storage period, because the NIR reflectance is higher in aged leaves and the reflectance at 540–560 nm is lower. Therefore the chlorophyll content is likely to increase, but this fact is impossible in harvested leaves. As it has been explained previously, the water content of the leaves decreases during time. These two facts allow to extract the hypothesis that there is an increase in the relative concentration of chlorophyll because of the water decreasing is higher than the chlorophyll decreasing which could cause the described effect on the spectra (Fig. 3, upper left).

On the mean spectra, a shift towards the left at the red edge region for the 21 testing days can be observed. Fig. 4 (right) shows this more clearly. The loadings of the PC3 of the radiometric corrected spectra (Fig. 3, lower left) shows a big peak in the range be-

[1] For interpretation of color in Fig. 3, the reader is referred to the web version of this article.

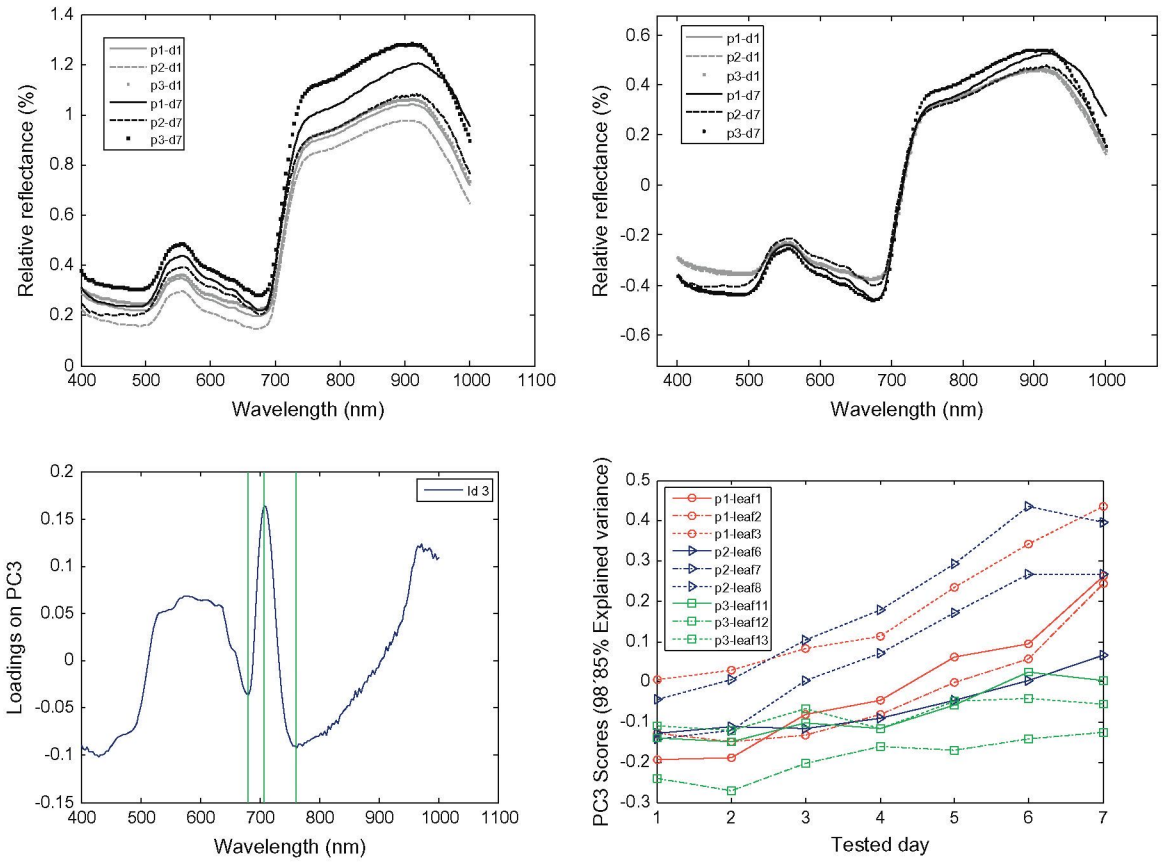

Fig. 3. Upper left: mean radiometric corrected spectra of the leaves of each plastic (p1, p2, p3), on the calibration set, on first (d1) and last date (d7). Upper right: mean centered spectra of the same leaves. Lower left: PC3 loading from PCA applied on mean radiometric corrected spectra. Lower right: scores of PC3 on mean spectra of the leaves of calibration set along the time.

Table 2
Spectral bands maximally sensitive to absorption by main pigments. Adapted by Gitelson et al. (2006).

Pigment	Wavelength range (nm)
Chlorophylls in anthocyanins free leaves (<3 mg/m^2)	540–560 690–720
Chlorophylls in leaves containing anthocyanins	690–720
Carotenoids	510–520
Anthocyanins	540–560

tween 680 and 760 nm, with its maximum at 707 nm. So PC3 could be related to the evolution of red-edge of the leaves. Vertical lines mark the most relevant wavelengths of the loadings at the red edge range: 680, 707 and 760 nm. The same wavelengths are marked on the mean spectra (Fig. 4, right). Those wavelengths delimit the characteristic sharp change in the spectra at red-edge region for leafy vegetables, 707 nm could be near the inflection point.

Loadings of PC3 compute an approximation to the minus second derivative at 707 nm (-SD$_{707}$):

$$-\mathrm{SD}_{707} = 2 \cdot R_{707} - R_{680} - R_{760}$$

Second derivative is related to the curvature at 707 nm: if this wavelength corresponds to the inflection point, the $-\mathrm{SD}_{707}$ is equal to zero; on the contrary $-\mathrm{SD}_{707}$ will be positive if the spectrum is shifting towards the left and negative if the spectrum is shifting towards the right (Fig. 4, left). Fig. 3 (lower right) shows an increase in the values of the scores for the samples along time, which is consistent with the displacement of the spectra to the left on the red edge region.

Several studies have reported that, when leaves are aging and chlorophyll content decreases, red edge suffers a displacement towards shorter wavelengths (Mutanga and Skidmore, 2007; Van der Meer and Jong, 2002); therefore red edge could be used as a measurement for estimating the leaf chlorophyll content. Most of the reviewed and studied optical indexes include wavelengths from the red-edge region (Xue and Yang, 2009).

The analysis of the loadings of the PC3 on the NIR region (Fig. 3, lower left) allows identifying an approach to the calculation of the slope of the spectra between 760 and 1000 nm. Increasing slopes at the NIR range of the spectra along the evolution are reflected on increasing values of scores of PC3 (Fig. 3, lower right). This fact is in accordance with Asner (1998) who showed that, during aging, the slope of the spectra in the NIR region changes, becoming higher in dead leaves than in healthy leaves.

3.2.2. Smoothed and second derivative spectra

Fig. 5 (upper left) shows the mean spectra of the leaves subjected to RC and SG algorithm for each plastic on the first and the last days. The second derivative spectra of the reflectance spectra exhaust the absorbances as positive peaks. Thus, the main chlorophyll peak clearly appears around 680 nm in Fig. 5 (upper). In Fig. 5, the second highest peak appears around 510 nm and may be attributed to carotenoids (Gitelson et al., 2006 and Table 2). The third one, around 585 nm, should also be attributed to chlorophyll (Kleima et al., 2000). In these plots, it can be observed that chlorophyll and carotenoid peaks have slight increase in the values on the last day, whilst the peak at 585 nm does not change.

In the PCA performed on these spectra, PC1 was the most related one to the evolution of the leaves. The pre-processing of

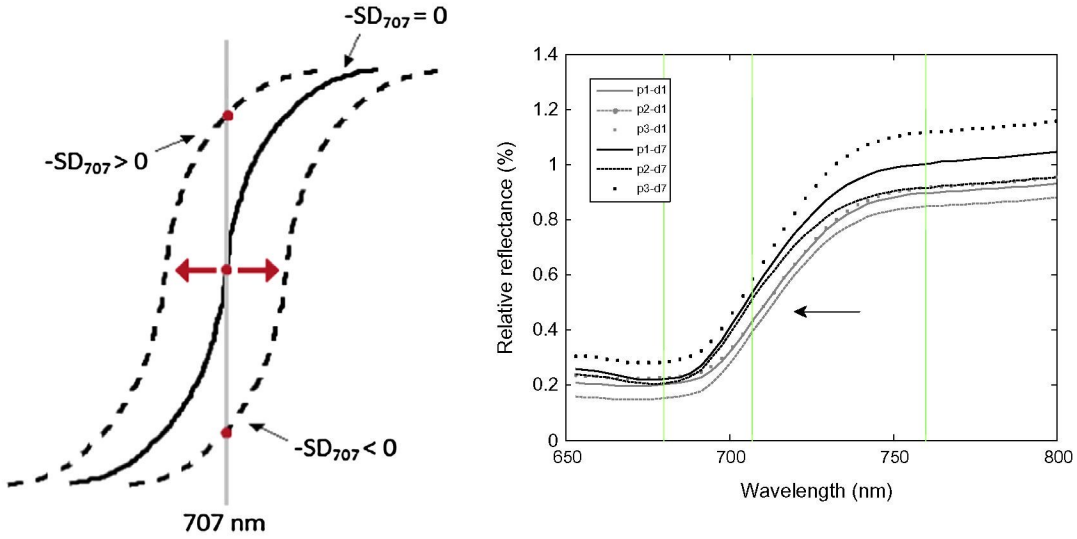

Fig. 4. Left: lateral movements of spectra on red-edge region cause changes in the values of minus second derivative (-SD). Right: detailed range of the spectra on red-edge region. (For interpretation of the references to color in this figure legend, the reader is referred to the web version of this article.)

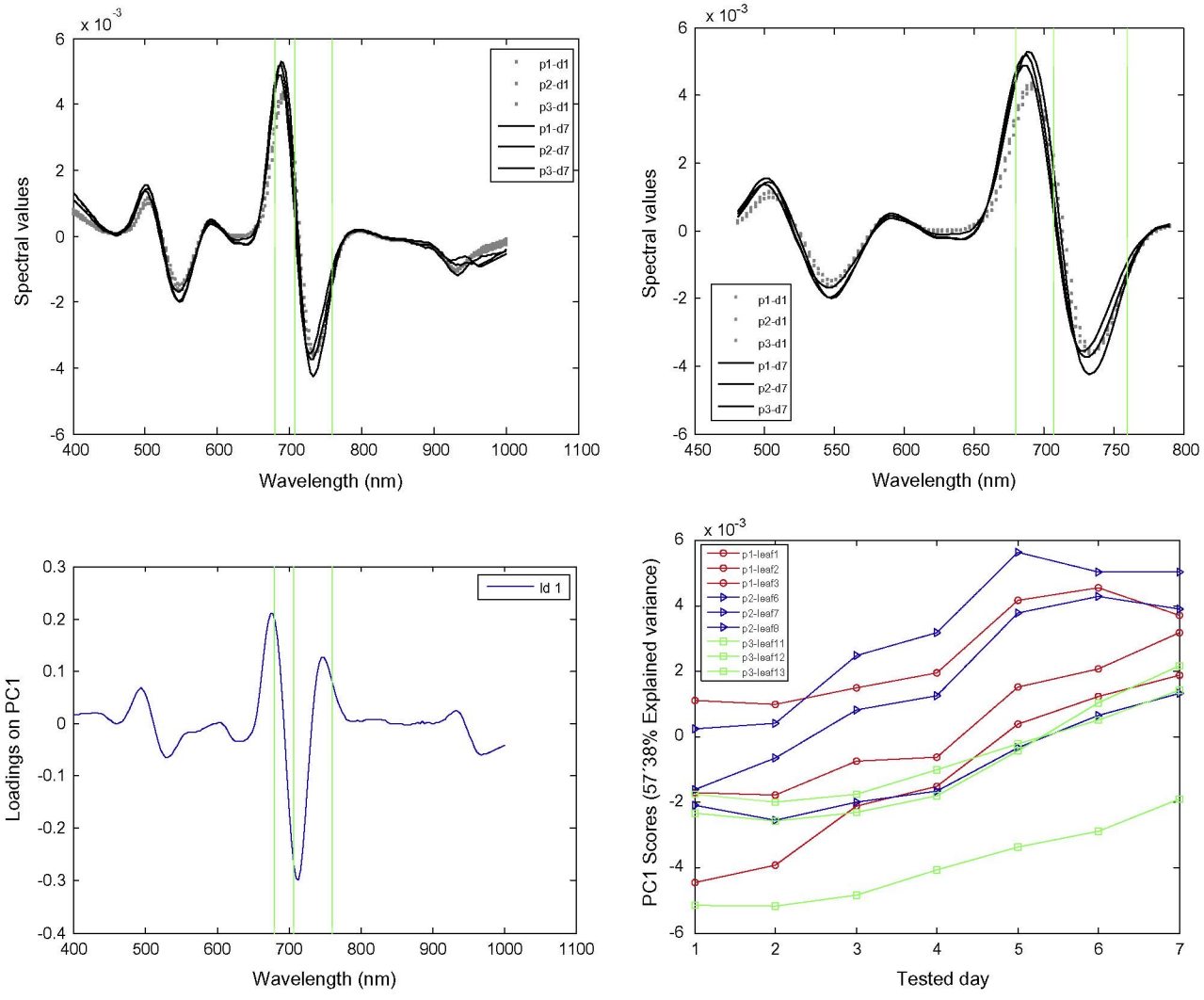

Fig. 5. Upper left: mean radiometric corrected, second derivative spectra of the leaves of each plastic, on first and last date. Upper right: detailed range of the spectra in which the differences are relevant. Lower left: PC1 loading from PCA applied on RC plus second derivative corrected spectra. Lower right: scores of PC1 on mean spectra of the leaves of calibration set along testing time.

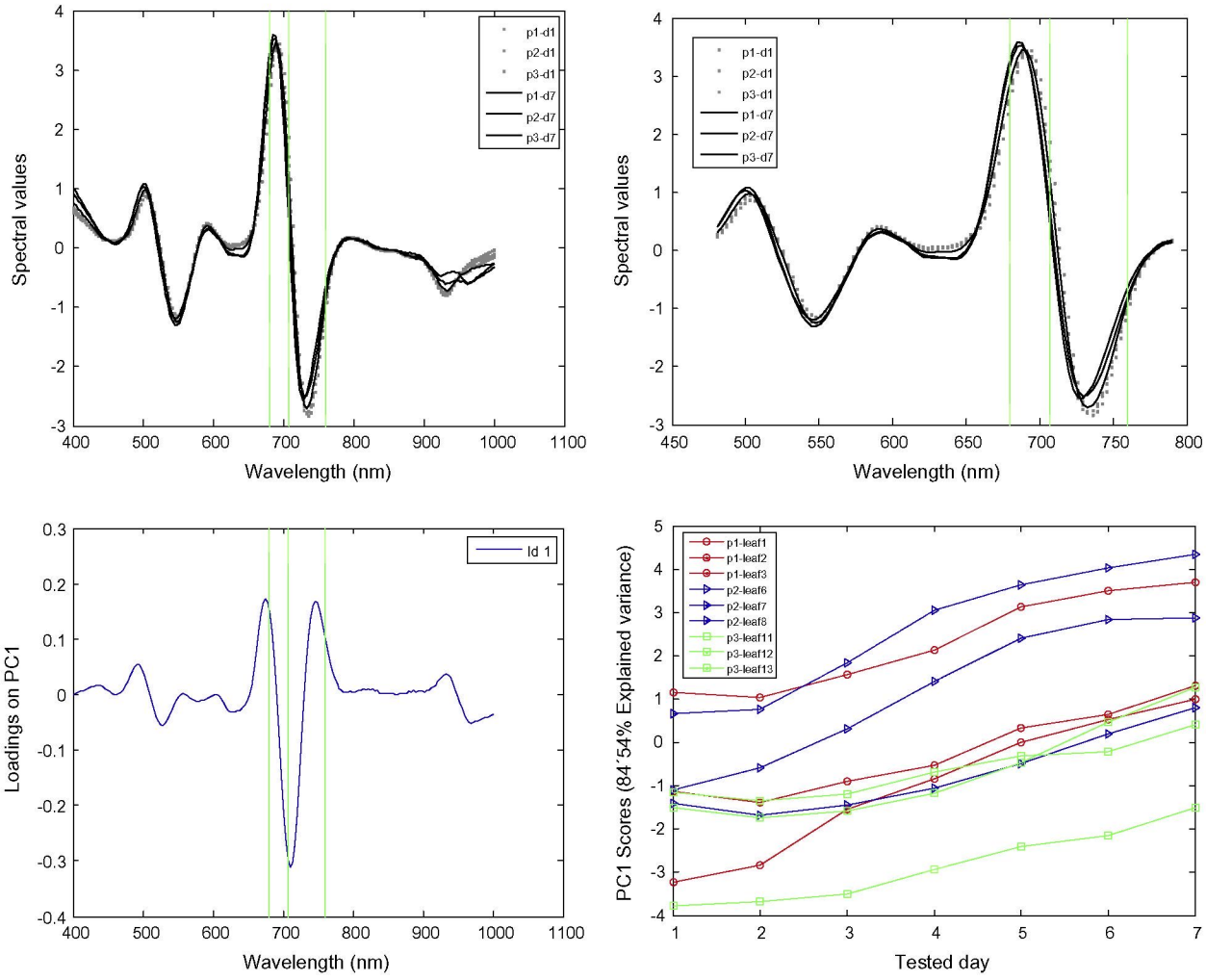

Fig. 6. Upper left: mean radiometric corrected, second derivative and SNV corrected spectra of the leaves of each plastic, on first and last date. Upper right: detailed range of the spectra. Lower left: PC1 loading from PCA applied on RC plus second derivative and SNV corrected spectra. Lower right: scores of PC1 on mean spectra of the leaves of calibration set at first and last day. Vertical green lines mark the wavelengths 680, 707 and 760 nm, delimiting the sharp change in the spectra at red-edge region. (For interpretation of the references to color in this figure legend, the reader is referred to the web version of this article.)

the spectra by means of SG algorithm seems to reduce the un-modeled information since the first score is directly related to the evolution of the leaves during time. The scores increased during the measurement period (Fig. 5, lower right).

The loadings reported in Fig. 5 (lower left), in association with the evolution of the corresponding scores, (Fig. 5 lower right), are in accordance with the preceding findings:

- Two clear positive peaks in correspondence with the chlorophyll and carotenoids peaks.
- A quite flat shape in the 585 nm area.

Moreover, the combination of the large negative peak at 710 nm and the positive one at 750 nm denotes a shift of the negative peak at 725 nm, noticeable in Fig. 5 (upper left). This peak corresponds to the end of the red edge of the reflectance spectra. Thus, the loadings sense in this area the red edge shift, as mentioned before.

Water has maximum absorptions centered near 1400 and 1900 nm, moreover water also has absorption bands centred on 970 nm and 1190 nm. However, the water peak at 970 nm does not appear in the second derivative spectra (Fig. 5, upper left), which could be due to the fact that this range corresponds to the less sensitive area of the hyperspectral detector.

3.2.3. Smoothed, second derivative and SNV spectra

Fig. 6 (upper left) shows the same mean spectra with additional SNV pre-treatment. It can be observed that the differences in the spectra between first and last day nearly disappear. SNV seems to produce loss of information regarding the evolution of the leaves during time.

On the corresponding PCA, again the PC1 was the most related to the evolution of the leaves. Once more, wavelengths around 680, 707 and 760 nm showed the highest values in the loadings.

It can be observed that the same shape appears in loadings of PC1 of RC plus SG (Fig. 5, lower left) and in loadings of PC1 of RC plus SG plus SNV (Fig. 6, lower left), but inverse that the corresponding loadings of PC3 of RC, because second derivative shows absorption zones as positive peaks.

3.3. Data processing

3.3.1. ANOVAs for the comparison of the preprocessing procedures

Results of ANOVA's performed on the scores of the artificial images to test the efficiency of the pre-processing are shown in Table 3.

In all the pre-processed images a significant evolution of the scores along the time could be observed (Table 3). According to the lowest F of Fisher in ANOVA's, the pre-processing procedure

Table 3
Analysis of variance comparing the scores of leaves at first date with the scores of leaves at last date, on each data set and on each data pre-processing. The scores considered for each case were PC3 scores for RC spectra; PC1 for RC plus SG and PC1 for RC plus SG plus SNV. Highest *F*-Fisher values are marked in bold characters.

		RC	RC + SG	RC + SG + SNV
Calibration set $n = 31{,}000$	*F*-Fisher	30,784	**38,997**	26,956
	p-level	0	0	0
Validation set $n = 17{,}000$	*F*-Fisher	**31,878**	19,225	14,199
	p-level	0	0	0
Calib. + Valid. set $n = 48{,}000$	*F*-Fisher	**59,141**	56,786	40,324
	p-level	0	0	0

including SNV could be the less sensitive to the evolution of the samples for the three sets of data. Multiplicative effect seems to be meaningful. Probably because multiplicative effect is related to scattering, which is due to changes of refractive indexes between cells and interstitial air.

Comparing the *F* values for RC and RC plus SG algorithm, it could not be concluded which procedure was the most segregating one. On validation set and on calibration plus validation set the RC showed the highest *F* value; on the contrary, the RC plus SG algorithm presented the highest *F* of Fisher on the calibration set.

As a result of the previous ANOVÁs and in order to implement the simplest preprocessing procedures, only samples with RC were taken into account for further analysis.

Results of ANOVA's performed to evaluate the goodness of the plastics are shown in Table 4. Considering the *F* of Fisher values, it could be concluded that leaves under plastic 1 presented the highest evolution; consequently, it could be noted that, on this experimental design, plastic 1 showed the worst behavior on the preservation of leaves. On the other hand, the lowest *F* value of plastic 3 could indicate the best behavior of this covering material. Plastic 2 showed an intermediate behavior.

Table 4
Analysis of variance comparing the scores of the leaves at first date with the scores of the leaves at last date, on each cover plastic and on each data set. The considered scores were resulting of the projection of RC spectra onto PC3.

		Plastic 1	Plastic 2	Plastic 3
Calibration set $n = 7400$	*F*-Fisher	35,014	22,530	3,230
	p-level	0	0	0
Validation set $n = 3900$	*F*-Fisher	11,048	10,481	6,258
	p-level	0	0	0

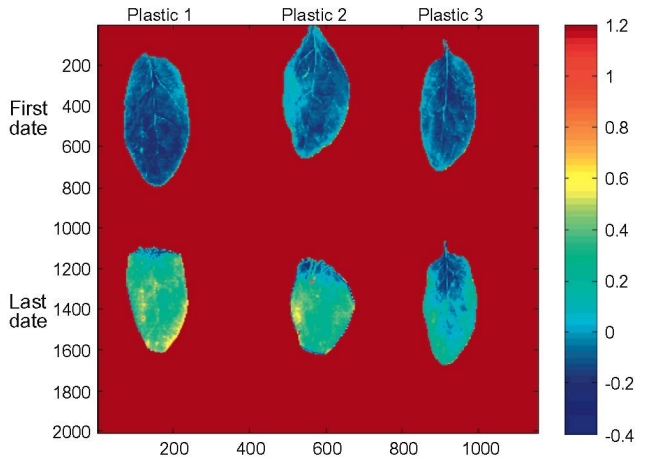

Fig. 7. Scores images obtained by projection of the hyperspectral radiometric corrected images on PC3. It is shown one leaf of each plastic from the validation set: left to right plastic 1, plastic 2 and plastic 3. Upper: first date. Lower: last date.

Table 5
Analysis of variance comparing the scores of each individual leaf at first and last date, and average values of the leaves with the same plastic on calibration and on validation sets.

	Number of leaf	Plastic film	*F*-Fisher	Average *F*-Fisher
Calibration set $n = 800$	*1*	1	13,536	7453
	2		5379	
	3		3444	
	6	2	1909	7233
	7		12,899	
	8		6890	
	11	3	722	524
	12		756	
	13		95	
Validation set $n = 800$	*4*	1	9074	5755
	5		2437	
	9	2	3494	2033
	10		572	
	14	3	994	1373
	15		1752	

Results of ANOVA's computed on the scores of individual leaves are shown in Table 5. In general, regarding the average values of *F* of Fisher, the same conclusions as in previous analyses (Table 4) about the behavior of plastic films could be drawn. However, individual *F* values presented differences between leaves covered with the same plastic films. It could denote that the evolution rate was different for each leaf, and the initial freshness stage could be variable even in leaves belonging to the same commercial bag.

Fig. 7 shows scores images obtained by the projection of the RC hyperspectral images on PC3. One representative leaf of each plastic from the validation set on the first and last day is included. Differences among the three types of packing plastic appear clearly, in accordance with the results from ANOVÁs (Tables 4 and 5); leaf under plastic 3 presented less evolution, and leaf under plastic 1 showed higher evolution rate. Remaining scores images (computed

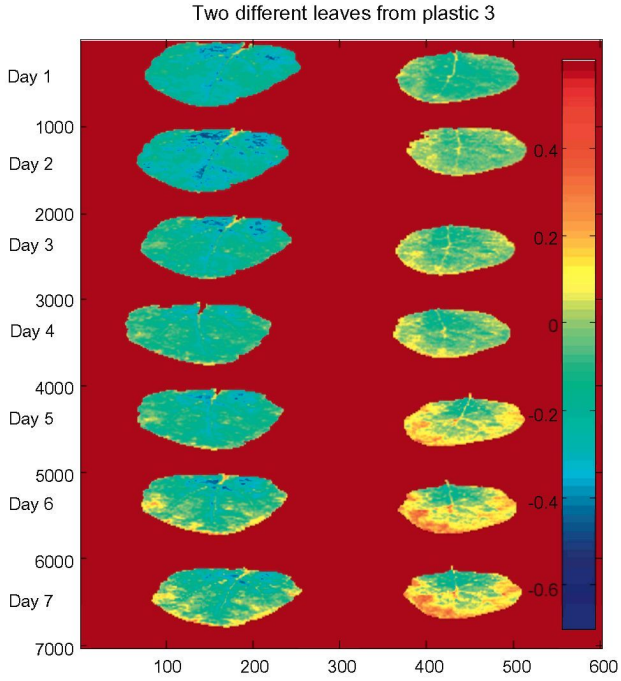

Fig. 8. Virtual image of loading 3 from the radiometric corrected data PCA. Two different leaves from plastic 3 on the seven tested days.

for all considered pre-processing procedures) were congruent regarding plastic behavior identification: plastic 1 seems to be the worst type for protecting spinach leaves since their leaves evolved mainly in the score images (images not shown). Similar results are presented in Figs. 4–6 (lower right), where the scores for plastic 3 during the time of the study experimented less evolution (see green lines).

Fig. 8 illustrates the differences in the evolution rate and in the initial freshness stage of the leaves. Two leaves under plastic 3 are monitored through the storage. Evolution was apparently more intense in the periphery of the leaf. In the region near the peduncle, the evolution was lower. Additionally, veins of the leaves seemed to be more resistant to the evolution (lower scores values). It can be observed that the initial freshness stage of each leaf is very different.

4. Conclusions

The present research focused on the use of hyperspectral images (400–1000 nm) in spinach, under three commercial packaging plastic films, to monitor their evolution during storage (21 days, 4 °C). Different pre-processing procedures were applied to the images (radiometric correction, Savitsky Golay algorithm, and Standard Normal Variate combined with a principal component analysis).

The effect of the variation of the transmittance of the plastic on the spectra of leaves was removed applying radiometric correction to the hyperspectral images. Therefore this procedure may allow the monitoring of shelf-life in leafy vegetables through packaging transparent films.

The main changes observed on the spectra of spinach during storage period were: the shift of the red-edge to shorter wavelengths probably due to aging in leaves, as Van der Meer and Jong (2002) described before; the increase in the global reflectance, mainly in the infrared region, probably due to changes in the structure of the leaves and loss of water (Jacquemoud and Baret, 1990); and the increase in the slope of the spectra at the infrared region due to the aging of leaves, as Asner (1998) stated.

A methodology for the evaluation of the different pre-processing procedures was proposed. ANOVA results show that all procedures were able to monitor the loss of freshness of the spinach leaves during the storage, although radiometric correction presented slight better performance in their ability to discriminate evolution stages.

Moreover, the behavior of the plastic films along the storage period was evaluated for their ability to slow the loss of freshness. Remarkable variability on initial freshness stage and evolution rate was verified in leaves belonging to the same batch of packages, which indicates the advantages that could be gained if an image analysis system is applied to obtain an overall quality assessment of packaged products.

Further analysis has to be conducted to compare the effect of plastic films in the preservation of the leaves. To validate the obtained results, an extended analysis with an increased sample size will be necessary. The challenge for the next step of this research is the definition of multispectral indexes based on the loadings obtained from PCAs and on the pattern of the spectra, capable of following the evolution during storage and removing the effect of the plastic films.

Acknowledgements

The funding of this work has been covered by the MICINN with the project Multihort (AGL2008-05666-C02-01) and by the Technical University of Madrid with de project Durasfrut II (AL11-P(I+D)-06). LPF-TAGRALIA is part of the CEI Moncloa Campus.

References

Artes, F., Gomez, P., Aguayo, E., Escalona, V., Artes-Hernandez, F., 2009. Sustainable sanitation techniques for keeping quality and safety of fresh-cut plant commodities. Postharvest Biology and Technology 51 (3), 287–296.

Asner, G.P., 1998. Biophysical and biochemical sources of variability in canopy reflectance. Remote Sensing of Environment 64 (3), 234–253.

Cubero, S., Aleixos, N., Molto, E., Gomez-Sanchis, J., Blasco, J., 2011. Advances in machine vision applications for automatic inspection and quality evaluation of fruits and vegetables. Food and Bioprocess Technology 4 (4), 487–504.

del Fiore, A., Reverberi, M., Ricelli, A., Pinzari, F., Serranti, S., Fabbri, A.A., Bonifazi, G., Fanelli, C., 2010. Early detection of toxigenic fungi on maize by hyperspectral imaging analysis. International Journal of Food Microbiology 144 (1), 64–71.

Du, C.J., Sun, D.W., 2006. Learning techniques used in computer vision for food quality evaluation: a review. Journal of Food Engineering 72 (1), 39–55.

Elmasry, G., Sun, D., 2010. Chapter 1 – principles of hyperspectral imaging technology. In: Sun, Da-Wen (Ed.), Hyperspectral Imaging for Food Quality Analysis and Control. Academic Press, San Diego, pp. 3–43.

Fearn, T., Riccioli, C., Garrido-Varo, A., Guerrero-Ginel, J.E., 2009. On the geometry of SNV and MSC. Chemometrics and Intelligent Laboratory Systems 96 (1), 22–26.

Fernandez Pierna, J.A., Baeten, V., Dardenne, P., Dubois, J., Lewis, E.N., Burger, J., 2009. Spectroscopic imaging. In: A2ROMÀ Tauler, Stephen D. Brown, Walczak, Beata (Eds.), Comprehensive Chemometrics. Elsevier, Oxford, pp. 173–196.

Garcia Gimeno, R.M., Zurera Cosano, G., 1997. Determination of ready-to-eat vegetable salad shelf-life. International Journal of Food Microbiology 36 (1), 31–38.

Gitelson, A.A., Keydan, G.P., Merzlyak, M.N., 2006. Three-Band Model for Noninvasive Estimation of Chlorophyll Carotenoids and Anthocyanin Contents in Higher Plant Leaves. Papers in Natural Resources. Paper 258. <http://digitalcommons.unl.edu/natrespapers/258>.

Gowen, A.A., O'Donnell, C.P., Cullen, P.J., Downey, G., Frias, J.M., 2007. Hyperspectral imaging – an emerging process analytical tool for food quality and safety control. Trends in Food Science and Technology 18 (12), 590–598.

Jacquemoud, S., Baret, F., 1990. Prospect – a model of leaf optical-properties spectra. Remote Sensing of Environment 34 (2), 75–91.

Kleima, F.J., Wendling, M., Hofmma, E., Peterman, E.J.G., Van Grondelle, R., Van Amerongen, H., 2000. Peridinin chlorophyll *a* protein: relating structure and steady-state spectroscopy. Biochemistry 39, 5184–5195.

Laxalde, J.R.M., Ruckebusch, C., Devos, O., Caillol, N.M., Wahl, F.O., Duponchel, L., 2011. Characterisation of heavy oils using near-infrared spectroscopy: optimisation of pre-processing methods and variable selection. Analytica Chimica Acta 705, 227–234.

Liy, Z.Y., Shi, J.J., Wang, D.C., Huang, J.F., 2010. Discrimination and spectral response characteristic of stress leaves infected by rice *Aphelenchoides besseyi* Christie. Guang Pu Yu Guang Pu Fen Xi. Spectroscopy and Spectral Analysis 30 (3), 710–714.

Mutanga, O., Skidmore, A.K., 2007. Red edge shift and biochemical content in grass canopies. ISPRS Journal of Photogrammetry and Remote Sensing 62 (1), 34–42.

Pavia, D.L., Lampman, G.M., Kriz, G.S., Engel, R.G., 2007. Introduction to Organic Laboratory Techniques: A Microscale Approach, fourth ed. Tomson Books, Cole, UK.

Rinnan, A., van den Berg, F., Engelsen, S.B., 2009. Review of the most common pre-processing techniques for near-infrared spectra. Trac-Trends in Analytical Chemistry 28 (10), 1201–1222.

Sims, D.A., Gamon, J.A., 2002. Relationships between leaf pigment content and spectral reflectance across a wide range of species, leaf structures and developmental stages. Remote Sensing of Environment 81 (2–3), 337–354.

Siripatrawan, U., Makino, Y., Kawagoe, Y., Oshita, S., 2011. Rapid detection of *Escherichia coli* contamination in packaged fresh spinach using hyperspectral imaging. Talanta 85 (1), 276–281.

Song, C., Woodcock, C.E., Seto, K.C., Lenney, M.P., Macomber, S.A., 2001. Classification and change detection using Landsat TM data: when and how to correct atmospheric effects? Remote Sensing of Environment 75 (2), 230–244.

Sun, T., Huang, K., Xu, H., Ying, Y., 2010. Research advances in nondestructive determination of internal quality in watermelon/melon: a review. Journal of Food Engineering 100 (4), 569–577.

Toivonen, P.M.A., Brummell, D.A., 2008. Biochemical bases of appearance and texture changes in fresh-cut fruit and vegetables. Postharvest Biology and Technology 48 (1), 1–14.

Van der Meer, F.D., Jong, S.M., 2002. Imaging spectrometry: basic principles and prospective applications. Remote Sensing and Digital Image Processing 4, 113–135 (Springer. Chapter 5).

Xue, L., Yang, L., 2009. Deriving leaf chlorophyll content of green-leafy vegetables from hyperspectral reflectance. ISPRS Journal of Photogrammetry and Remote Sensing 64 (1), 97–106.

Yao, H., Hruska, Z., Kincaid, R., Brown, R.L., Cleveland, T.E., 2008. Differentiation of toxigenic fungi using hyperspectral imagery. Sensing and Instrumentation for Food Quality and Safety 2, 215–224.

Zeaiter, M., Rutledge, D., 2009. Preprocessing methods. In: A2ROMÀTauler, Stephen D. Brown, Walczak, Beata (Eds.), Comprehensive Chemometrics. Elsevier, Oxford, pp. 121–231.

Zeaiter, M., Roger, J.M., Bellon-Maurel, V., 2005. Robustness of models developed by multivariate calibration. Part II: The influence of pre-processing methods. Trac-Trends in Analytical Chemistry 24 (5), 437–445.